PAPER

Check for updates

Visible optical nonlinearity of vanadium dioxide dispersions

Longlong Chen, Jing Huang, Qian Yi, Dongyang Liu, Yuan He, Ning Li, Yi Feng, Lili Miao and Chujun Zhao [ID] *

Vanadium dioxide (VO_2), a correlated oxide compound, is one of the functional materials extensively studied in solid state physics due to its attractive physical properties. However, the nonlinear optical response of VO_2 and related all-optical applications have been paid less attention. Here, the nonlinear refractive index (n_2) and third-order nonlinear susceptibility ($\chi^{(3)}$) of VO_2 dispersions have been acquired to be 3.06×10^{-6} cm^2 W^{-1} and 1.68×10^{-4} esu at a wavelength of 671 nm, and 5.17×10^{-6} cm^2 W^{-1} and 2.83×10^{-4} esu at a wavelength of 532 nm *via* the spatial self-phase modulation (SSPM) and spatial cross-phase modulation (SXPM) effects in the visible regime, respectively. Based on the excellent nonlinear optical properties of VO_2 dispersions, the proof-of-principle functions such as optical logic or-gates, all-optical switches, and inter-channel information transfer are implemented in the visible wavelength. The experimental results on the response time of VO_2 to light indicate that the formation of diffraction rings is mainly an electronically coherent third-order nonlinear optical process. The experimental results show that the VO_2 dispersions exhibit an excellent nonlinear optical response and may lay the foundation for the application of VO_2-based all-optical devices.

1. Introduction

All-optical modulation, a light-control-light scheme analogous to its counterpart of electronic modulation, plays an important role in signal processing, such as multiplexing and demultiplexing, signal regeneration, and optical logic gates.[1,2] Usually, all-optical modulation can be achieved by utilizing the third-order nonlinear response of optical material or the thermo-optic effect *via* waveguide or free-space configurations.[3–5] By comparison with the waveguide-based optical modulation, the free-space ones can realize broadband, high-power and high efficiency optical modulation, not limited by the availability of the low-loss waveguides.[6]

The all-optical modulation can be demonstrated by the SSPM and SXPM effects in free space.[7,8] The SSPM effect is a coherent third-order nonlinear optical process observed in liquid crystals in 1981.[9] Subsequently, the phenomenon was also noticed in other materials, such as ferrofluid,[10] $Sr_xBa_{1-x}Nb_2O_6$ and $BaTiO_3$ crystal,[11] and carbon nanotube.[12] In 2011, Wu *et al.* studied the SSPM effect of two-dimensional graphene.[13] Then, the SSPM effect was also discovered for many two-dimensional materials.[4,8,14–16] In 2015, Wu *et al.* studied the SXPM effect of two-dimensional MoS_2 for the first time and

achieved an all-optical switch, showing that the SXPM effect is a typical all-optical modulation or all-optical control technique that enables light-to-light control.[17] Subsequently, the SXPM effect of various two-dimensional materials has been studied successively, demonstrating the modulation and processing of optical signals.[18–21] However, the performance of the all-optical device is limited by the physiochemical properties of the optical material, such as the stability and the optical nonlinearity. Two-dimensional materials have some common problems, such as poor stability, easy oxidation, and low threshold of optical damage, which can weaken the optical performance of materials. To avoid these drawbacks, it is necessary to find optical materials with excellent performance in other dimensions.

VO_2 is one of the most widely explored functional materials in solid state physics given its attractive physical properties.[22–24] Based on the characteristics of VO_2, researchers have implemented devices that can actively modulate the performance by external excitation, such as cloaking device[25,26] and active metasurface.[27,28] In addition, the refractive index of VO_2 changes by orders of magnitude during the structural change, which provides the possibility of dynamic adjustment of the optical system.[29] The ultrafast response of VO_2 to light is accompanied by a considerable number of photoexcited carriers, which makes it a candidate material for photodetector and photo-transistor applications.[30] The excellent properties of VO_2 have made it widely used in the field of optics and optoelectronics, such as reversible all-optical switch,[31] memorizer,[32] adjustable optical polarization state system,[33] memory metamaterial[34] and

Key Laboratory for Micro-/Nano-Optoelectronic Devices of Ministry of Education, Hunan Provincial Key Laboratory of Low-Dimensional Structural Physics and Devices, School of Physics and Electronics, Hunan University, Changsha 410082, China. E-mail: cjzhao@hnu.edu.cn

optical driver.[35] However, the nonlinear optical response of VO_2 and related applications, especially in the visible spectrum range, have been paid less attention.

Here, we studied the nonlinear optical response of VO_2 dispersions using the SSPM and SXPM effects and demonstrated their all-optical applications in the visible range. The n_2 and $\chi^{(3)}$ of the VO_2 dispersions have been extracted at the incident wavelengths of 671 nm and 532 nm, respectively. It is found that the nonlinear optical response of VO_2 dispersions can be modulated by the SXPM effect, which is beneficial to meet the needs of different optical applications. In addition, VO_2-based all-optical applications in the visible spectral have been experimentally demonstrated, including the optical logic or-gate, all-optical switch, and inter-channel information transfer device. Furthermore, the response time of the SXPM effect suggests that the formation of diffraction rings of VO_2 dispersions is mainly an electronically coherent third-order nonlinear optical process.

2. Material preparation and characterization

The VO_2 particles are obtained from Macklin Biochemical Technology Co. The particles are ground and dissolved in *N*-methylpyrrolidone (NMP), and the concentration of the solution is 0.6 mg mL^{-1}. Fig. 1(a) shows the energy band diagram of VO_2 calculated with the first principle. The figure indicates that the bandgap of VO_2 is about 0.57 eV, which means that the VO_2 can respond to the visible light. Fig. 1(b) shows the X-ray diffraction (XRD) pattern of the samples with the peak positions corresponding to JCPDS codes 18-1445 ($VO_2 \cdot xH_2O$) and 09-0142 (VO_2), indicating that the composition of the samples is VO_2, and the inset shows the molecular structure of VO_2. Fig. 1(c) shows the linear transmission spectra of the samples, and the curve follows the same trend as the VO_2 thin films.[28,36] Fig. 1(d), (e) and (f) show the energy dispersive spectroscopy (EDS) characterization of the samples, indicating that only V

and O elements are present in the samples and that both elements are uniformly distributed in the samples. The atomic ratio of V to O is 36 : 64, which is about 1 : 2 and is consistent with the atomic ratio of VO_2. The transmission electron microscopy (TEM) characterization of samples is shown in Fig. 1(g). The photograph clearly displays the lattice fringes of samples, indicating the crystalline nature of the samples. The lattice spacing is measured to be about 3.21 Å, which is consistent with the reported results.[37] Fig. 1(h) shows the scanning electron microscope (SEM) photograph of samples, which shows that the grain size of particles is about several hundred nanometers. The inset of Fig. 1(h) displays the selected area electron diffraction (SAED) characterization of samples, which indicates that the samples are polycrystalline.

3. Results and discussion

3.1 Nonlinear optical response of vanadium dioxide dispersions

3.1.1 SSPM effect of the vanadium dioxide dispersions. The SSPM effect is a manifestation for the nonlinear optical response of materials like other nonlinear optical processes.[13] The schematic diagram for observing the SSPM effect is shown in the inset of Fig. 2(a). The light sources used in the experiments are red light (671 nm) and green light (532 nm) with continuous-wave operation. The laser beam is focused by lens and irradiated to the VO_2 dispersions. The nonlinear optical response of the samples is manifested in the far field, displayed as diffraction rings on a screen or charge-coupled device (CCD). As shown in Fig. 2, the laser beam expands into circular rings within a short time after passing through the dispersions, in which both the bright and dark stripes gradually widen from the centre of the circle outward. The correspondence between the light intensity of the two beams and the number of diffraction rings is shown in Fig. 2(a). As can be seen from the figure, the intensity of two beams shows a linear relationship with the number of diffraction rings, and the slope of green light is larger than that of red light. Fig. 2(b) shows the diffraction rings
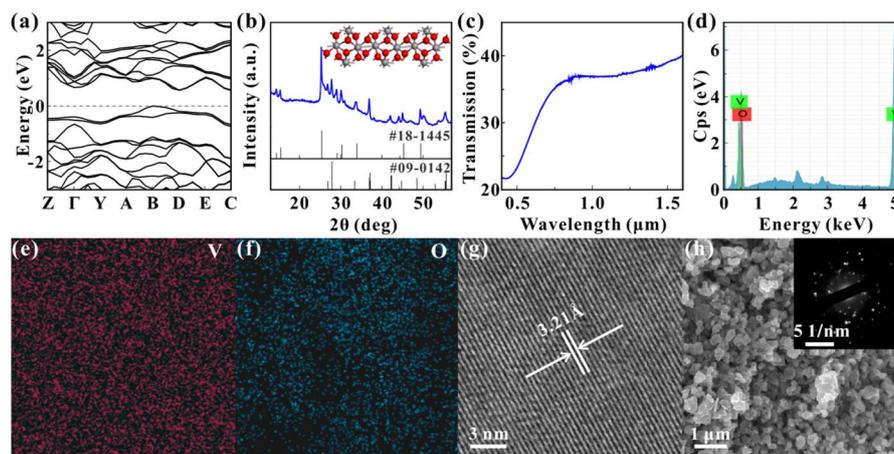

Fig. 1 Material characterizations. (a) Energy band diagram of VO_2. (b) XRD pattern. The inset is the molecular structure of VO_2. (c) Linear transmission spectrum. (d) EDS diagram. (e) and (f) EDS mappings of V and O. (g) TEM image. (h) SEM image. The inset is the SAED image.
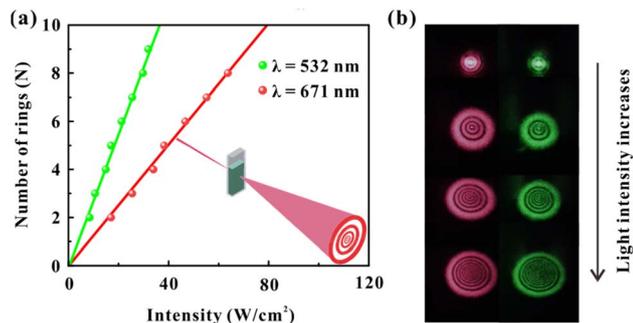
Fig. 2 SSPM effect of the VO$_2$ dispersions. (a) Correspondence between the incident intensity and the number of diffraction rings. The inset is schematic diagram for observing the SSPM effect. (b) The diffraction rings vary with increasing incident intensity.

of two beams, which correspond to a gradual increase in the light intensity from top to bottom. It can be seen from the figure that both the diameter and the diffraction ring number increase with the increasing incident intensity. In order to exclude the influence of the solvent, the same operation has been performed with the solvent only, and no diffraction rings can be observed.

The interaction between light and VO$_2$ dispersions can excite diffraction rings. When the Gaussian light passes through the samples, the phase shift $\Delta\psi$ of the light is expressed as,[38]

$$\Delta\psi = \frac{2\pi n_0}{\lambda} \int_0^{L_{\text{eff}}} n_2 I(r, z)\mathrm{d}z, \ r \in [0, +\infty) \quad (1)$$

where n_0 is the linear refractive index, λ is the wavelength of the incident light, L_{eff} is the effective transmission distance of the incident light, and n_2 is the nonlinear refractive index. r and $I(r, z)$ are the radial coordinates and the intensity distribution of the incident light, respectively. L_{eff} is expressed as,[4]

$$L_{\text{eff}} = \int_{L_1}^{L_2} \left(1 + \frac{z^2}{z_0^2}\right)^{-1} \mathrm{d}z = z_0 \arctan\left(\frac{z}{z_0}\right)\Big|_{L_1}^{L_2}, \ z_0 = \frac{\pi\omega_0^2}{\lambda} \quad (2)$$

where L_1 and L_2 are the distances from the focal point of the incident light being focused by the lens in the optical path to the front and back of the quartz cuvette, respectively. z_0 is the Rayleigh length of the laser beam, ω_0 is the waist radius. n_2 can be expressed as,[39]

$$n_2 = \frac{\lambda}{2n_0 L_{\text{eff}}} \cdot \frac{N}{I} \quad (3)$$

where N and I are the number of diffraction rings and the incident intensity, respectively. $\chi^{(3)}$ is expressed as,[4]

$$\chi^{(3)} = \frac{10^{-4} \varepsilon_0 n_0^2 c^2}{\pi} \cdot n_2 \quad (4)$$

where ε_0 is the vacuum dielectric constant, and c is the speed of light in vacuum. With the above calculations, the n_2 is about 3.06×10^{-6} cm^2 W^{-1} and $\chi^{(3)}$ is about 1.68×10^{-4} esu when VO$_2$ dispersions are irradiated by laser with the wavelength of 671 nm. The n_2 is about 5.17×10^{-6} cm^2 W^{-1} and $\chi^{(3)}$ is about 2.83×10^{-4} esu when the dispersions are irradiated by laser with the wavelength of 532 nm.

3.1.2 SXPM effect of the vanadium dioxide dispersions. Two beams of light will interact with each other along their propagation through a nonlinear optical material.[40] An experimental setup is designed to realize the light-to-light control, as shown in the inset of Fig. 3(a). Two monochromatic lights are focused by the lens in the VO$_2$ dispersions to induce the SXPM effect. Here, the intensity change of the control light can affect the diffraction ring number of the probe light, that is, the control light can affect the phase of the probe light.[20,41]

The light-control-light experimental results are shown in Fig. 3. Fig. 3(a) and (b) show the results of red light (control light) control of green light (probe light). The intensity of two monochromatic lights is low at the beginning (red: 4.3 W cm^{-2}, green: 7.4 W cm^{-2}), and lasers show only Gaussian spots when passing through the dispersions. Then, by only gradually increasing the intensity of the red beam (the intensity of the green beam is always 7.4 W cm^{-2} and remains constant), two colors of diffraction rings can be observed in the far field due to the SXPM effect. Fig. 3(a) shows the correspondence between the intensity of red light and the number of green diffraction rings, and Fig. 3(b) shows the correspondence between the number of rings for two beams and their incident intensity. The figures show that the ring number of green light is linearly related to the intensity of red light. Moreover, the ring number of red light still shows a linear relationship with the intensity of the red light. The inset in Fig. 3(b) shows the diffraction rings for two beams, which correspond to the gradual increase in intensity of red light from top to bottom. It can be seen from the
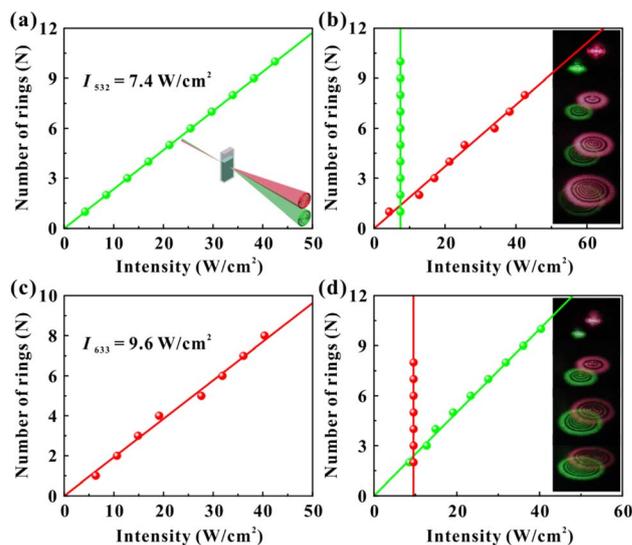

Fig. 3 SXPM effect of the VO$_2$ dispersions. (a) Correspondence between the intensity of red light and the number of green diffraction rings, the inset is schematic diagram for observing the SXPM effect. (b) Correspondence between the number of rings for the two beams and the respective incident intensity. The inset shows the variation of the diffraction rings with increasing intensity of red beam from top to bottom. (c) Correspondence between the intensity of green light and the number of red rings. (d) Correspondence between the number of two diffraction rings and the respective incident intensity. The inset shows the variation of the diffraction rings with increasing intensity of green beam from top to bottom.

figures that both the diameter and the ring number of two beams increase as the intensity of red light (control light) increases. Fig. 3(c) and (d) show the experimental results of the green light control of red light. The intensity of red light remains constant (9.6 W cm^{-2}), and only the intensity of green light gradually increases. The figures show that the diffraction ring number of two beams is linearly related to the intensity of green light, which is similar as the experimental results in Fig. 3(a) and (b).

3.1.3 Modulation of the nonlinear optical response of vanadium dioxide dispersions by the SXPM effect.

The dN/dI is an important optical parameter to evaluate the nonlinear optical response of the nonlinear optical materias.[18,38,42] However, the investigation on the relationship between the dN/dI and the nonlinear optical response of optical materials has mainly focused on the SSPM effects,[4,14,16,19,20,43] not the SXPM case. Here, we studied the nonlinear optical response of VO$_2$ dispersions in the SXPM effect. Fig. 4(a) and (b) show the correspondence between the sum of incident intensity and the diffraction ring number in the SXPM effect with red and green light used as control light, respectively. From the figures, the ring numbers of both control light and probe light are linearly related to the sum of incident intensity. When the monochromatic light irradiates the dispersions (see Fig. 2), dN_{532}/dI_{532} = 0.28 cm^2 W^{-1} and dN_{671}/dI_{671} = 0.13 cm^2 W^{-1}. This indicates that the nonlinear response is stronger when the dispersion is irradiated with green light than with red light.[18,38,41,44] In the SXPM effect, dN_{671}/dI_{sum} = 0.18 cm^2 W^{-1} and 0.20 cm^2 W^{-1}, and dN_{532}/dI_{sum} = 0.24 cm^2 W^{-1} and 0.26 cm^2 W^{-1}. The values of 0.18 cm^2 W^{-1} and 0.20 cm^2 W^{-1} for the nonlinear optical response of the dispersions at 671 nm (dN_{671}/dI_{sum}) are greater than 0.13 cm^2 W^{-1} (dN_{671}/dI_{671}), which can be explained by the stronger absorption of green light than the red light. Likewise, the values of 0.24 cm^2 W^{-1} and 0.26 cm^2 W^{-1} for the nonlinear optical response of the dispersions at 532 nm (dN_{532}/dI_{sum}) are smaller than 0.28 cm^2 W^{-1} (dN_{532}/dI_{532}), which can be explained by the modulation of the red light.

With the above experimental results, the modulation of nonlinear optical response of dispersions can be achieved by taking advantage of the interaction between red and green light in the SXPM effect. Here, the nonlinear optical response of red light to the samples is modulated from an initial 0.13 cm^2 W^{-1} to 0.18 cm^2 W^{-1} and 0.20 cm^2 W^{-1}, while the nonlinear optical
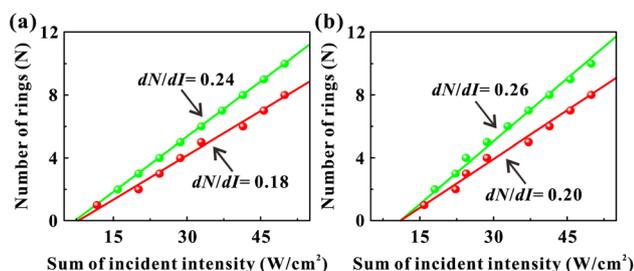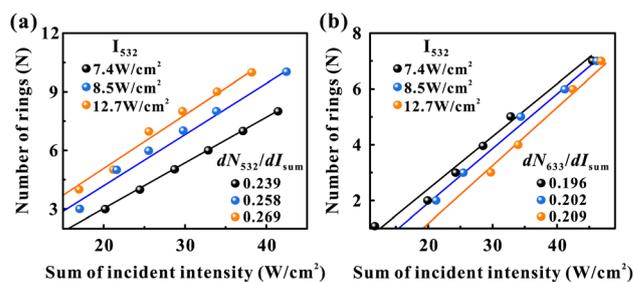

Fig. 5 Correspondence between the number of diffraction rings and the sum of incident intensity for the SXPM effect of the VO$_2$ dispersions. (a) The variation pattern of dN_{532}/dI_{sum}. (b) The variation pattern of dN_{633}/dI_{sum}. The black data, blue data, and orange data represent the green light intensity as 7.4 W cm^{-2}, 8.5 W cm^{-2} and 12.7 W cm^{-2}, respectively.

response of green light to the samples is modulated from an initial 0.28 cm^2 W^{-1} to 0.24 cm^2 W^{-1} and 0.26 cm^2 W^{-1}. The method of modulating the nonlinear optical response of the VO$_2$ dispersions by SXPM effect may enable on-demand modulation of the nonlinear optical response of materials.

In the SXPM effect, we keep the intensity of the green light constant at 7.4 W cm^{-2} and vary the intensity of the red light (see Fig. 3(a) and (b)). Here, we vary the intensity of the green light and study the variation of dN/dI. As shown in Fig. 5, the black data, blue data, and orange data represent the green light intensity as 7.4 W cm^{-2}, 8.5 W cm^{-2} and 12.7 W cm^{-2}, respectively. Fig. 5(a) represents the variation pattern of dN_{532}/dI_{sum}, from which it can be seen that dN_{532}/dI_{sum} increases slightly as the green light intensity increases. Fig. 5(b) represents the variation pattern of dN_{633}/dI_{sum}, from which it can be seen that dN_{633}/dI_{sum} also increases slightly as the light intensity of green light increases. This can also be explained by the fact that the absorption of green light is stronger than that of red light, and an increase in the intensity of green light will also modulate red light more strongly.

3.2 All-optical applications based on vanadium dioxide dispersions

3.2.1 Optical logic or-gate based on vanadium dioxide dispersions.

All-optical logic gates are the most fundamental logic units in all-optical systems, which are the basis of optical computing and play an important role in signal processing. An optical logic or-gate is implemented by utilizing the designed light-control-light device, as shown in Fig. 6. Fig. 6(a) and (b) indicate the electrical logic or-gate and the corresponding truth table, respectively. Analogous to the logic gate in electricity, the incident light cannot excite the diffraction rings defined as 0 (low level) and can excite the diffraction rings defined as 1 (high level). As shown in Fig. 6(c), columns A and B indicate the patterns of diffraction rings when red and green monochromatic light is irradiated to the dispersions, respectively. Column Y shows the patterns when both light beams are irradiated to the dispersions. The experimental results are comparable to the logic or-gate in electricity. That is, the output (Y) is 1 when the input (A and B) of either channel is 1, and the
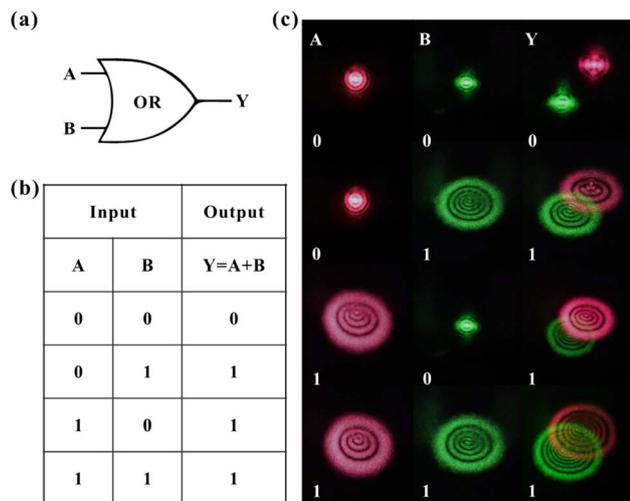

Fig. 4 Correspondence between the number of diffraction rings and the sum of incident intensity for the SXPM effect of the VO$_2$ dispersions. (a) The control light is red light. (b) The control light is green light.

Fig. 6 Logic or-gate based on the VO₂ dispersions. (a) Electrical logic or-gate. (b) Truth table of electrical logic or-gate. (c) Experimental results of optical logic or-gate.

output is 0 when the input of both channels is 0, as shown in Fig. 6(b) and (c). Therefore, the designed device implements the optical logic or-gate based on VO₂ dispersions. The VO₂-based logic gates require low incident power and low power consumption with simple and highly stable configuration. In addition, the logic gates can operate in broadband regime based on the broadband optical response of the VO₂.

3.2.2 All-optical switch based on vanadium dioxide dispersions. The diffraction rings undergo a gradual collapse process in their top half after reaching their maximum diameter.[13,17] Thus, the collapse process can be used to generate an all-optical switch. Here, we focus on the outermost diffraction ring, as shown in the dashed box in Fig. 7(a), which shows the collapse process of diffraction rings. The collapse process of the outermost diffraction ring takes about 33 ms and continues to
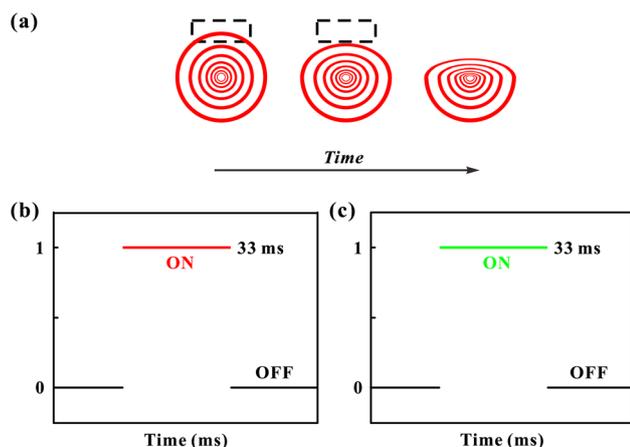
collapse until stabilization. Due to the collapse of diffraction rings, the height of rings decreases, which means that after the collapse, the dashed box changes from having a ring to having no ring. Therefore, the process can be regarded as an optical switch that lasts for 33 ms. Fig. 7(b) represents the optical switch generated with red light, and the "ON" state of the switch is the state of the red diffraction ring in the dashed box, and the "OFF" state is the state where there is no diffraction rings in the dashed box. The green optical switch has been studied, and the collapse time of the outermost ring is also found to be about 33 ms, which means that the diffraction rings generated with green light have the same effect of all-optical switch, as shown in Fig. 7(c).

3.2.3 Inter-channel information transmission based on vanadium dioxide dispersions. The schematic diagram of the inter-channel information transmission device is shown in Fig. 8. As can be seen from the figure, a small aperture is opened on the screen to transmit part of light from the green diffraction rings. A power meter is positioned behind the aperture to detect the light passing through it. The input of information is achieved by manipulating the control light. Fig. 8(a) shows that when the control light (red light) is closed, there are no diffraction rings (the intensity of green light is too low to excite the diffraction rings). That is, there is no green light through the aperture, and thus the power meter shows 0. Fig. 8(b) shows that when the control light is open, the diffraction rings of both light beams can occur due to the SXPM effect. Thus, part of the green light can pass through the aperture, and the power meter will detect this part of light.

Fig. 8(c) and (d) show the experimental results of inter-channel information transmission. Firstly, the power of red light (control light) is kept at 60 mW and the green light (probe
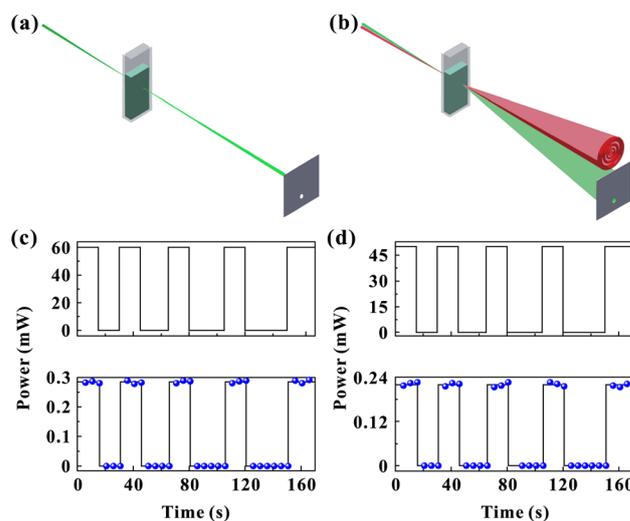
Fig. 8 Inter-channel information transmission with the VO₂ dispersions. (a) Red light is closed. (b) Red light is open. (c) The input information introduced through the red channel (upper). The information is obtained by measuring the green channel pass through the aperture (lower). (d) The input information introduced through the green channel (upper). The information is obtained by measuring the red channel pass through the aperture (lower).

Fig. 7 All-optical switch based on the VO₂ dispersions. (a) Schematic diagram of the collapse process for diffraction rings. (b) The optical switch generated by the red light. (c) The optical switch generated by the green light.

light) power at 7 mW (the green beam cannot excite diffraction rings at such a power). The red light is closed for 15, 20, 25, and 30 s all at 15 s intervals. Fig. 8(c) shows the power corresponding to time for red light and the power corresponding to time for green light passing through the aperture, respectively. As can be seen from the figure, the information curve of the green light (green channel) is the same as the red light (red channel), which means that the information transmitted by control light can be obtained by detecting the probe light.

Then, the power of the green beam is kept at 55 mW and the power of the red beam at 9 mW (red light at such a power cannot excite the diffraction rings). A similar experimental operation is performed, intermittently close the green light (input) while recording the power of red light (output) passing through the aperture, as shown in Fig. 8(d). The figure shows that the information curves of the green channel and the red channel are essentially the same, indicating the inter-channel information transmission function.

3.3 Diffraction rings formation as an electronically coherent nonlinear optical processes: a study of the response time

There are two prevailing views on the formation mechanism of diffraction rings: mainly thermal nonlinear effects[11,45,46] or mainly electronic coherence nonlinear effects.[13,17,20,47] Here, we experimentally verify by the response time that electronic coherence should play a major role in the VO$_2$ dispersions. During the experiment of SSPM effect, the response time is defined as the time required from the appearance of diffraction rings to their maximum diameter.[48,49] Fig. 9(a) represents the incident intensity corresponding to the response time for two monochromatic lights irradiating the dispersions (SSPM effect). The shortest response time in the experiment is about 0.36 s, as shown in Fig. 9(a), which is shorter than the response time of most two-dimensional materials.[16,19,43] The response time T is expressed as,[17]

$$T = \frac{\varepsilon_r \pi \eta \xi r c}{1.72(\varepsilon_r - 1)Ih} \quad (5)$$

where ε_r is the dielectric constant, η is the viscosity of the solvent, ξ is the compensation value, c is the speed of light in

vacuum, I is the incident intensity, r and h are the radius and thickness of the particles, respectively. It can be seen from eqn (5) that for the identical dispersions, the response time is inversely proportional to the incident intensity. The experimental results in Fig. 9(a) show that the response time decreases with the increase of the incident intensity in the SSPM effect, which is in accordance with the trend in eqn (5). However, the response time of the VO$_2$ dispersions is not significantly related to the incident intensity when the SXPM effect occurs, as shown in Fig. 9(b). It can be seen from the figure the response time does not decrease with the increase in incident intensity when two monochromatic lights are used as control light, respectively. Moreover, the response time has only small fluctuations and the trend remains flat overall, which is different from the trend of the response time for SSPM effect in Fig. 9(a). The response time is about 0.297–0.33 s (for λ = 671 nm) and 0.264–0.297 s (for λ = 532 nm) when the SXPM effect occurs. Compared with the results of SSPM effect in Fig. 9(a), the response time is shorter when the SXPM effect occurs. In addition, it is found experimentally that the formation process of diffraction rings at two wavelengths is synchronized when the SXPM effect occurs, regardless of which beam is used as the control light, which is consistent with the reported result.[50]

As the incident intensity increases, the temperature of the dispersions also increases. However, the experimental results in Fig. 9(b) show that the response time does not vary with the increase of the incident intensity. Thus, our results suggest that the formation of diffraction rings should be mainly attributed to electronically coherence nonlinear effects in VO$_2$ dispersions. According to the "wind-bell" model,[17] the suspended particles are polarized when the laser irradiates the dispersions, then the suspended particles tend to reorient from the disordered orientation to the electric field direction, as shown in Fig. 10. Thus, the response time of the SSPM effect is the time required from disordered orientation of the suspended particles under electric field to the completion of orientation, which can be shown as "Step one" in Fig. 10.

In the study of the SXPM effect, it is necessary to implement the control light (strong light) to modulate the probe light (weak light). The SSPM effect has a short response time of a few hundred milliseconds, so that the orientation (Step one) of the suspended particles due to the probe light is actually completed
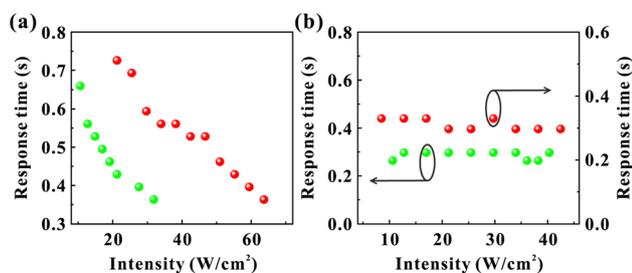

Fig. 9 Correspondence between the response time and the incident intensity of the VO$_2$ dispersions. (a) Response time for the SSPM effect. Two beams of monochromatic light are irradiated to the dispersions respectively. (b) Response time for the SXPM effect. The red light and green light are used as control light respectively.
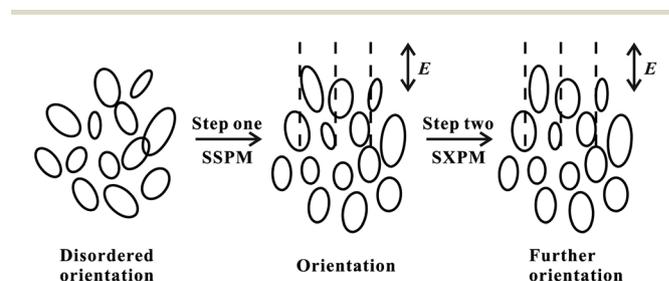

Fig. 10 The orientation process of the suspended particles. Step one: the response process of the SSPM effect. Step two: the response process of the SXPM effect. E: the direction of electric field.

before the control light irradiation to the VO$_2$ dispersions. When the control light is irradiated to the dispersions, the suspended particles need to complete further orientation under the stronger field. That is, the response time of the SXPM effect is the time required from control light irradiation to the dispersions to the completion of further orientation of the suspended particles, which can be shown as "Step two" in Fig. 10. In the SSPM effect, the large orientation angle between the disorderly oriented particles and the electric field, together with the viscous force of the solution, requires a certain amount of time to complete the orientation of the suspended particles. In the case of the SXPM effect, the orientation of the suspended particles is already quite close to the direction of the electric field, because the irradiation of the probe light causes the suspended particles tend to the direction of the electric field (Step one in Fig. 10). Therefore, a small orientation angle and viscous forces need to be overcome under stronger control light irradiation in order to complete further orientation for the suspended particles (Step two in Fig. 10), and thus the time required for this process is relatively short.

4. Conclusions

In conclusion, the interaction between light and VO$_2$ dispersions has been studied utilizing the SSPM and SXPM effects in the visible light regime. The dispersions exhibit excellent optical properties and promising nonlinear optical response. The n_2 and $\chi^{(3)}$ of VO$_2$ dispersions are measured to be 3.06×10^{-6} cm^2 W^{-1} and 1.68×10^{-4} esu at $\lambda = 671$ nm, and 5.17×10^{-6} cm^2 W^{-1} and 2.83×10^{-4} esu at $\lambda = 532$ nm, respectively. Due to the excellent nonlinear optical response of VO$_2$ dispersions, optical logic or-gate, optical switch, and inter-channel information transmission in visible regime have been implemented. The band gap of VO$_2$ is about 0.6 eV, indicating the broadband response of the VO$_2$-based optical modulators. In addition, the VO$_2$ dispersion can be used to realize the broadband, high-power and high efficiency all-optical modulation with simple experimental configuration. The response time indicates that the diffraction rings are mainly formed by an electronically coherent third-order nonlinear optical process. The findings contribute to a better understanding of the nonlinear optical response of VO$_2$ and may lay the foundation for their applications in all-optical devices. All-optical devices require low loss, high efficiency, miniaturization and high integration for practical applications, and thus our all-optical devices need to be designed and optimized in such direction.

Conflicts of interest

There are no conflicts to declare.

Acknowledgements

Notes and references

1 M. Hochberg, T. Baehr-Jones, G. Wang, M. Shearn, K. Harvard, J. Luo, B. Chen, Z. Shi, R. Lawson and P. Sullivan, *Nat. Mater.*, 2006, **5**, 703–709.

2 Z. Shi, L. Gan, T. Xiao, H. Guo and Z. Li, *ACS Photonics*, 2015, **2**, 1513–1518.

3 P. B. Deotare, I. Bulu, I. W. Frank, Q. Quan, Y. Zhang, R. Ilic and M. Loncar, *Nat. Commun.*, 2012, **3**, 846.

4 J. Yi, J. Li, S. Huang, L. Hu, L. Miao, C. Zhao, S. Wen, V. N. Mochalin and A. M. Rao, *InfoMat*, 2020, **2**, 601–609.

5 Z. Shi, J. Gong, J. Zhang, P. Xu, N. Yao, W. Fang, P. Wang, X. Guo and L. Tong, *ACS Photonics*, 2020, **7**, 2571–2577.

6 S. Yu, X. Wu, Y. Wang, X. Guo and L. Tong, *Adv. Mater.*, 2017, **29**, 1606128.

7 Y. Dong, S. Chertopalov, K. Maleski, B. Anasori, L. Hu, S. Bhattacharya, A. M. Rao, Y. Gogotsi, V. N. Mochalin and R. Podila, *Adv. Mater.*, 2018, **30**, 1705714.

8 G. Wang, S. Zhang, X. Zhang, L. Zhang, Y. Cheng, D. Fox, H. Zhang, J. N. Coleman, W. J. Blau and J. Wang, *Photonics Res.*, 2015, **3**, A51–A55.

9 S. D. Durbin, S. M. Arakelian and Y. R. Shen, *Opt. Lett.*, 1981, **6**, 411–413.

10 S. Pu, X. Chen, L. Chen, W. Liao, Y. Chen and Y. Xia, *Appl. Phys. Lett.*, 2005, **87**, 021905.

11 M. Horowitz, R. Daisy, O. Werner and B. Fischer, *Opt. Lett.*, 1992, **17**, 475–477.

12 W. Ji, W. Chen, S. Lim, J. Lin and Z. Guo, *Opt. Express*, 2006, **14**, 8958–8966.

13 R. Wu, Y. Zhang, S. Yan, F. Bian, W. Wang, X. Bai, X. Lu, J. Zhao and E. Wang, *Nano Lett.*, 2011, **11**, 5159–5164.

14 J. Li, K. Yang, L. Du, J. Yi, J. Huang, J. Zhang, Y. He, B. Huang, L. Miao, C. Zhao and S. Wen, *Adv. Opt. Mater.*, 2020, **8**, 2000382.

15 S. Xiao, Y. Ma, Y. He, Y. Wang, H. Xin, Q. Fan, J. Zhang, X. Li, Y. Zhang, J. He and Y. Wang, *Photonics Res.*, 2020, **8**, 1725–1733.

16 L. Wu, X. Jiang, J. Zhao, W. Liang, Z. Li, W. Huang, Z. Lin, Y. Wang, F. Zhang, S. Lu, Y. Xiang, S. Xu, J. Li and H. Zhang, *Laser Photonics Rev.*, 2018, **12**, 1800215.

17 Y. Wu, Q. Wu, F. Sun, C. Cheng, S. Meng and J. Zhao, *Proc. Natl. Acad. Sci. U. S. A.*, 2015, **112**, 11800–11805.

18 L. Wu, Y. Dong, J. Zhao, D. Ma, W. Huang, Y. Zhang, Y. Wang, X. Jiang, Y. Xiang, J. Li, Y. Feng, J. Xu and H. Zhang, *Adv. Mater.*, 2019, **31**, 1807981.

19 Y. Jia, Y. Shan, L. Wu, X. Dai, D. Fan and Y. Xiang, *Photonics Res.*, 2018, **6**, 1040–1047.

20 L. Lu, W. Wang, L. Wu, X. Jiang, Y. Xiang, J. Li, D. Fan and H. Zhang, *ACS Photonics*, 2017, **4**, 2852–2861.

21 L. Wu, S. Wei, Y. Zhang, Y. Zhang, Y. Xiang, H. Zhang and Y. Qin, *Adv. Opt. Mater.*, 2022, **10**, 2102537.

22 F. J. Morin, *Phys. Rev. Lett.*, 1959, **3**, 34–36.

23 A. Zylbersztejn and N. F. Mott, *Phys. Rev. B*, 1975, **11**, 4383–4395.

24 A. Cavalleri, C. Tóth, C. W. Siders, J. A. Squier, F. Ráksi, P. Forget and J. C. Kieffer, *Phys. Rev. Lett.*, 2001, **87**, 237401.

25 L. Xiao, H. Ma, J. Liu, W. Zhao, Y. Jia, Q. Zhao, K. Liu, Y. Wu, Y. Wei, S. Fan and K. Jiang, *Nano Lett.*, 2015, **15**, 8365–8370.

26 S. Chandra, D. Franklin, J. Cozart, A. Safaei and D. Chanda, *ACS Photonics*, 2018, **5**, 4513–4519.

27 J. Rensberg, S. Zhang, Y. Zhou, A. S. McLeod, C. Schwarz, M. Goldflam, M. Liu, J. Kerbusch, R. Nawrodt, S. Ramanathan, D. N. Basov, F. Capasso, C. Ronning and M. A. Kats, *Nano Lett.*, 2016, **16**, 1050–1055.

28 T. Kang, Z. Ma, J. Qin, Z. Peng, W. Yang, T. Huang, S. Xian, S. Xia, W. Yan, Y. Yang, Z. Sheng, J. Shen, C. Li, L. Deng and L. Bi, *Nanophotonics*, 2021, **10**, 909–918.

29 M. Li, S. Magdassi, Y. Gao and Y. Long, *Small*, 2017, **13**, 1701147.

30 J. Lu, H. Liu, S. Deng, M. Zheng, Y. Wang, J. A. van Kan, S. Tang, X. Zhang, C. H. Sow and S. G. Mhaisalkar, *Nanoscale*, 2014, **6**, 7619–7627.

31 O. L. Muskens, L. Bergamini, Y. Wang, J. M. Gaskell, N. Zabala, C. H. de Groot, D. W. Sheel and J. Aizpurua, *Light: Sci. Appl.*, 2016, **5**, e16173.

32 D. Lei, K. Appavoo, F. Ligmajer, Y. Sonnefraud, R. F. Haglund and S. A. Maier, *ACS Photonics*, 2015, **2**, 1306–1313.

33 Z. Jia, F. Shu, Y. Gao, F. Cheng, R. Peng, R. Fan, Y. Liu and M. Wang, *Phys. Rev. Appl.*, 2018, **9**, 034009.

34 T. Driscoll, H. T. Kim, B. G. Chae, B. J. Kim, Y. W. Lee, N. M. Jokerst, S. Palit, D. R. Smith, M. Di Ventra and D. N. Basov, *Science*, 2009, **325**, 1518–1521.

35 T. Wang, D. Torres, F. E. Fernandez, A. J. Green, C. Wang and N. Sepulveda, *ACS Nano*, 2015, **9**, 4371–4378.

36 J. H. Yu, S. H. Nam, J. W. Lee, D. I. Kim and J. H. Boo, *Appl. Surf. Sci.*, 2019, **477**, 22–26.

37 K. L. Gurunatha, S. Sathasivam, J. Li, M. Portnoi, I. P. Parkin and I. Papakonstantinou, *Adv. Funct. Mater.*, 2020, **30**, 2005311.

38 L. Wu, W. Huang, Y. Wang, J. Zhao, D. Ma, Y. Xiang, J. Li, J. S. Ponraj, S. C. Dhanabalan and H. Zhang, *Adv. Funct. Mater.*, 2019, **29**, 1806346.

39 L. Wu, T. Fan, S. Wei, Y. Xu, Y. Zhang, D. Ma, Y. Shu, Y. Xiang, J. Liu, J. Li, K. Panajotov, Y. Qin and H. Zhang, *Opto-Electron. Adv.*, 2022, **5**, 200046.

40 L. Wu, X. Yuan, D. Ma, Y. Zhang, W. Huang, Y. Ge, Y. Song, Y. Xiang, J. Li and H. Zhang, *Small*, 2020, **16**, 2002252.

41 C. Song, Y. Liao, Y. Xiang and X. Dai, *Sci. Bull.*, 2020, **65**, 1030–1038.

42 X. Li, R. Liu, H. Xie, Y. Zhang, B. Lyu, P. Wang, J. Wang, Q. Fan, Y. Ma, S. Tao, S. Xiao, X. Yu, Y. Gao and J. He, *Opt. Express*, 2017, **25**, 18346–18354.

43 L. Wu, Z. Xie, L. Lu, J. Zhao, Y. Wang, X. Jiang, Y. Ge, F. Zhang, S. Lu, Z. Guo, J. Liu, Y. Xiang, S. Xu, J. Li, D. Fan and H. Zhang, *Adv. Opt. Mater.*, 2018, **6**, 1700985.

44 Y. Liao, Y. Shan, L. Wu, Y. Xiang and X. Dai, *Adv. Opt. Mater.*, 2020, **8**, 1901862.

45 S. Radha, S. Mohan and C. Pai, *Physica B*, 2014, **448**, 341–345.

46 S. Xiao, B. Lv, L. Wu, M. Zhu, J. He and S. Tao, *Opt. Express*, 2015, **23**, 5875–5887.

47 B. Shi, L. Miao, Q. Wang, J. Du, P. Tang, J. Liu, C. Zhao and S. Wen, *Appl. Phys. Lett.*, 2015, **107**, 151101.

48 S. Xiao, Y. Zhang, Y. Ma, Y. Wang, Y. He, J. Zhang, Y. Jiang, X. Li, R. Yang, J. He and Y. Wang, *Opt. Lett.*, 2020, **45**, 2850–2853.

49 L. Wu, Y. Zhang, X. Yuan, F. Zhang, W. Huang, D. Ma, J. Zhao, Y. Wang, Y. Ge, H. Huang, N. Xu, J. Kang, Y. Xiang, Y. Zhang, J. Li and H. Zhang, *Appl. Mater. Today*, 2020, **19**, 100589.

50 L. Lu, Z. Liang, L. Wu, Y. Chen, Y. Song, S. C. Dhanabalan, J. S. Ponraj, B. Dong, Y. Xiang, F. Xing, D. Fan and H. Zhang, *Laser Photonics Rev.*, 2018, **12**, 1700221.